Ar^+ ion milling rib waveguides on nonlinear optical (Yb,Nb):RTP/RTP epitaxial layers

J. Cugat,[1] A. Choudhary,[2] R. Solé,[1]* J. Massons,[1] D. Shepherd,[2] F. Díaz[1] and M. Aguiló[1]

[1] *Física i Cristal·lografia de Materials i Nanomaterials (FiCMA-FiCNA) and EMaS, Universitat Rovira i Virgili (URV), Marcel·lí Domingo s/n, Tarragona E-43007, Spain*

[2]*Optoelectronics Research Centre (ORC), University of Southampton, Southampton SO171BJ, UK*

** rosam.sole@urv.cat*

Abstract: In this paper we present the fabrication and characterization of rib waveguides made on (Yb,Nb):$RbTiOPO_4$/$RbTiOPO_4$ epitaxial layers. Liquid phase epitaxy (LPE) was used to grow planar thin films followed by Ar^+ ion milling for surface rib fabrication. Here, we report the detailed fabrication procedure and characterization of the ribs. The study reveals good optical confinement and that type II second harmonic generation inside the rib was obtained, showing the generation of green light at 570 nm.

OCIS codes: (190.4390) Nonlinear optics, integrated optics; (230.7370) Waveguides; (310.2790) Guided waves.

References and links

1. P. A. Thomas, S. C. Mayo, and B. E. Watts, "Crystal structures of $RbTiOAsO_4$, $KTiO(P_{0.56}As_{0.42})O_4$, $RbTiOPO_4$, and $(Rb_{0.465}K_{0.535})TiOPO_4$, analysis of pseudosymmetry in crystals of the $KTiOPO_4$," Acta Crystallogr. B **48**(4), 401–407 (1992).
2. R. F. Belt, G. Gashurov, and Y. S. Liu, "KTP as a harmonic generator for Nd:YAG lasers," Laser Focus **21**, 110 (1985).
3. C. Bibeau, R. J. Beach, S. C. Mitchell, M. A. Emanuel, J. Skidmore, C. A. Ebbers, S. B. Sutton, and K. S. Jancaitis, "High-average-power 1 μm performance and frequency conversion of a diode-end-pumped Yb:YAG laser," IEEE J. Quantum Electron. **34**(10), 2010–2019 (1998).
4. C. Zumsteg, J. D. Bierlein, and T. E. Gier, "$K_xRb_{1-x}TiOPO_4$: a new nonlinear optical material," J. Appl. Phys. **47**(11), 4980–4985 (1976).
5. R. Solé, V. Nikolov, I. Koseva, P. Peshev, X. Ruiz, C. Zaldo, M. J. Martín, M. Aguiló, and F. Díaz, "Conditions and possibilities for rare-earth doping of $KTiOPO_4$ flux-growth single crystals," Chem. Mater. **9**(12), 2745–2749 (1997).
6. J. J. Carvajal, R. Solé, J. Gavaldà, J. Massons, M. Aguiló, and F. Díaz, "Crystal growth of $RbTiOPO_4$:Nb. A new nonlinear host for rare earth doping," Cryst. Growth Des. **1**, 479–484 (2001).
7. X. Mateos, V. Petrov, A. Peña, J. J. Carvajal, M. Aguiló, F. Díaz, P. Segonds, and B. Boulanger, "Laser operation of Yb^{3+} in the acentric $RbTiOPO_4$ codoped with Nb^{5+}," Opt. Lett. **32**(13), 1929–1931 (2007).
8. Y. S. Oseledchik, A. I. Pisarevsky, A. L. Prosvirnin, V. V. Starshenko, and N. V. Svitanko, "Nonlinear optical properties of the flux grown $RbTiOPO_4$ crystal," Opt. Mater. **3**(4), 237–242 (1994).
9. Y. Guillen, B. Ménaert, J. P. Feve, P. Segonds, J. Douady, B. Boulanger, and O. Pacaud, "Crystal growth and refined Sellmeier equations over the complete transparency range of $RbTiOPO_4$," Opt. Mater. **22**(2), 155–162 (2003).
10. M. N. Satyanarayan, A. Deepthy, and H. L. Bhat, "Potassium titanyl phosphate and its isomorphs: growth, properties, and applications," Crit. Rev. Solid State Mater. Sci. **24**(2), 103–191 (1999).
11. T. Suhara and M. Fujimura, *Waveguide Nonlinear-Optic Devices* (Springer, 2003).
12. A. Peña, J. J. Carvajal, J. Massons, J. Gavaldà, F. Díaz, and M. Aguiló, "Yb:Ta:$RbTiOPO_4$ a new strategy to further increase the lanthanide concentration in cystals of the $KTiOPO_4$ family," Chem. Mater. **19**, 4069–4076 (2007).
13. J. Cugat, R. Solé, J. J. Carvajal, M. C. Pujol, X. Mateos, F. Díaz, and M. Aguiló, "Crystal growth and characterization of $RbTi_{1-x-y}Yb_xNb_yOPO_4$/$RbTiOPO_4$ (001) non-linear optical epitaxial layers," CrystEngComm **13**(6), 2015–2022 (2011).
14. J. Cugat, R. Solé, J. J. Carvajal, X. Mateos, M. C. Pujol, J. Massons, F. Díaz, and M. Aguiló, "Efficient Type II phase-matching second-harmonic generation in Ba:Yb:Nb:$RbTiOPO_4$/$RbTiOPO_4$ waveguides," Opt. Lett. **36**(10), 1881–1883 (2011).
15. W. Bolaños, J. J. Carvajal, X. Mateos, G. S. Murugan, A. Z. Subramanian, J. S. Wilkinson, E. Cantelar, D. Jaque, G. Lifante, M. Aguiló, and F. Díaz, "Mirrorless buried waveguide laser in monoclinic double tungstates fabricated by a novel combination of ion milling and liquid phase epitaxy," Opt. Express **18**(26), 26937–26945 (2010).

#194568 - $15.00 USD Received 25 Jul 2013; revised 26 Sep 2013; accepted 28 Sep 2013; published 21 Oct 2013

16. R. Solé, V. Nikolov, A. Vilalta, J. J. Carvajal, J. Massons, J. Gavaldà, M. Aguiló, F. Díaz, J. Gavaldà, M. Aguiló, and F. Díaz, "Liquid phase epitaxy of $KTiOPO_4$ on $KTi_{1-x}Ge_xOPO_4$ substrates," J. Cryst. Growth **237**, 602–607 (2002).
17. A. Aznar, O. Silvestre, M. C. Pujol, R. Solé, M. Aguiló, and F. Díaz, "Liqud phase epitaxy crystal growth of monoclinic $KLu_{1-x}Yb_x(WO_4)_2$ /$KLu(WO_4)_2$ layers," Cryst. Growth Des. **6**(8), 1781–1787 (2006).
18. W. Bolaños, J. J. Carvajal, M. C. Pujol, X. Mateos, G. Lifante, M. Aguiló, and F. Díaz, "Epitaxial growth of lattice matched $KY_{1-x-y}Gd_xLu_y(WO_4)_2$ thin films on $KY(WO_4)_2$ substrates for waveguiding applications," Cryst. Growth Des. **9**(8), 3525–3531 (2009).
19. W. P. Risk, S. D. Lau, R. Fontana, L. Lane, and Ch. Nadler, "Type II second harmonic generation and sum frequency mixing in uniform KTiOPO4 channel waveguides," Appl. Phys. Lett. **63**(10), 1301–1303 (1993).

1. Introduction

$RbTiOPO_4$ (RTP) is a nonlinear optical crystal that belongs to the $KTiOPO_4$ (KTP) family and crystallizes in the orthorhombic space group $Pna2_1$ [1]. Crystals of this family have been extensively used for frequency doubling infra-red (IR) laser radiation close to 1 μm, such as Yb^{3+} and Nd^{3+} laser emissions [2,3]. RTP has similar nonlinear optical coefficients to KTP [4], but unlike KTP, it can be doped with Yb^{3+} ions to a high enough concentration to allow efficient laser action [5–7]. Therefore, by combining the emission of Yb^{3+} with the nonlinear optical properties of the crystal, it is possible to obtain a self-frequency doubling material. RTP has other interesting properties, such as a high laser damage threshold, about 2 times larger than that of KTP [8,9], large electro-optical coefficients, low dielectric constants [10], high chemical stability and low photorefractive damage susceptibility [11]. Owing to all these interesting properties, RTP is a promising candidate as a platform material for integrated photonics.

Yb^{3+} has many advantages in comparison to other rare-earth ions. Its ionic radius is much closer to the radius of Ti^{4+} than the radius of other Ln^{3+} ions, which may be the cause of the higher distribution coefficient of Yb^{3+} in relation to other Ln^{3+} ions in the crystals of the KTP family [5]. Moreover, the Yb^{3+} ion has a simpler energy scheme than Nd^{3+} with a similar emission range in the IR region. The Yb^{3+} energy scheme consists of only two energy levels: the ground state $^2F_{7/2}$ and the exited state $^2F_{5/2}$. This is important since it avoids many effects that can lead to a reduction of the laser efficiency, such as excited-state absorption, cross-relaxation and up-conversion. The quantum defect, which leads to the thermal loading of the crystal during the laser operation, is very small in Yb^{3+} due to the similarity between the pumping and the laser wavelengths [12]. Moreover, the Yb^{3+} ion has no absorption losses at the second-harmonic generation frequency [7], which makes it interesting for self-frequency doubling.

Previously, (Yb,Nb):RTP planar waveguides were successfully fabricated on RTP substrates by the liquid phase epitaxy (LPE) technique [13], and efficient type II second harmonic generation (SHG) was obtained [14]. In this paper, we have used Ar^+ ion milling [15] to microstructure the surface of the epitaxial layers and obtain rib waveguides.

2. Experiments

In order to design the suitable width and depth of the channels, we have carried out a computer simulation using the Multi Grid Finite Difference (Real) method at 972 nm, with commercially available software (OlympIOs). This wavelength has been selected because, in previous works, it has been used to pump (Yb,Nb):RTP lasers [7]. The refractive indices of the epitaxial layer and the substrate used in the simulation were measured experimentally via the dark mode method, using a Metricon prism-coupler set-up and a Ti:sapphire laser. Table 1 shows the refractive index values obtained with an accuracy of 5×10^{-4}. In this work, only TM values were used corresponding to the n_z polarization. We simulated the ribs produced on a hypothetical planar waveguide with a thickness of 5 μm. The ribs were 3, 5 and 10 μm in width and 3 μm in depth. The confinement factor of the ribs, defined as the fraction of the mode intensity within the cross section of the rib area, was 40.0% for ribs of 3 μm in width, 83.3% for ribs of 5 μm in width, and finally 92.9% for ribs of 10 μm in width.

#194568 - $15.00 USD Received 25 Jul 2013; revised 26 Sep 2013; accepted 28 Sep 2013; published 21 Oct 2013

Table 1. Refractive index values at a wavelength of 972 nm and contrast of refractive indices between film and substrate.

	n_x (E//*a*)	n_y(E//*b*)	n_z (E//*c*)
substrate	1.7675	1.7774	1.8573
film	1.7649	1.7778	1.8631
$\Delta n = n_{film}-n_{sub}$	–0.0026	0.0004	0.0058

With the aim of obtaining planar waveguides with a thickness of 5 µm, we grew epitaxial layers of (Yb,Nb):RTP on (001) oriented RTP substrates. The planar substrates, which were 1.5 mm in thickness, with faces perpendicular to the ***c*** crystallographic direction, were cut from bulk RTP single crystals. The ***a-b*** plane is interesting because it contains the non-critical phase matching (PM) type II SHG directions for the range of 985 to 1118 nm, moreover the Yb^{+3} laser emission at 1060 nm is in this range. To grow the epitaxial layers we used the LPE technique from WO_3-containing solutions. Rb_2CO_3 (99%), $NH_4H_2PO_4$ (99%), TiO_2 (99.9%), Yb_2O_3 (99.9%), Nb_2O_5 (99.9%) and WO_3 (99.9%) were used as starting chemicals. The fabrication procedure has been previously reported [16–18]. The solution composition was Rb_2O-P_2O_5-TiO_2-Yb_2O_3-Nb_2O_5-WO_3 = 43.9-23.6-20.7-1.35-0.45-10 (mol %). The saturation temperature of the solution was around 1153 K and the growth process started by producing supersaturation on cooling the solution 2 K below the saturation temperature. During the growth process a rotation of 60 rpm was applied. The chemical composition of the epitaxial layers was determined by electron probe microanalysis (EPMA) with a final result of $RbTi_{0.958}Yb_{0.016}Nb_{0.026}OPO_4$. The thickness of the as-grown epitaxial layers, measured by an interferometric microscope was around 50 µm. The epitaxial layer was then polished down to a thickness of 5 µm to obtain a planar waveguide which supported a small number of propagation modes.

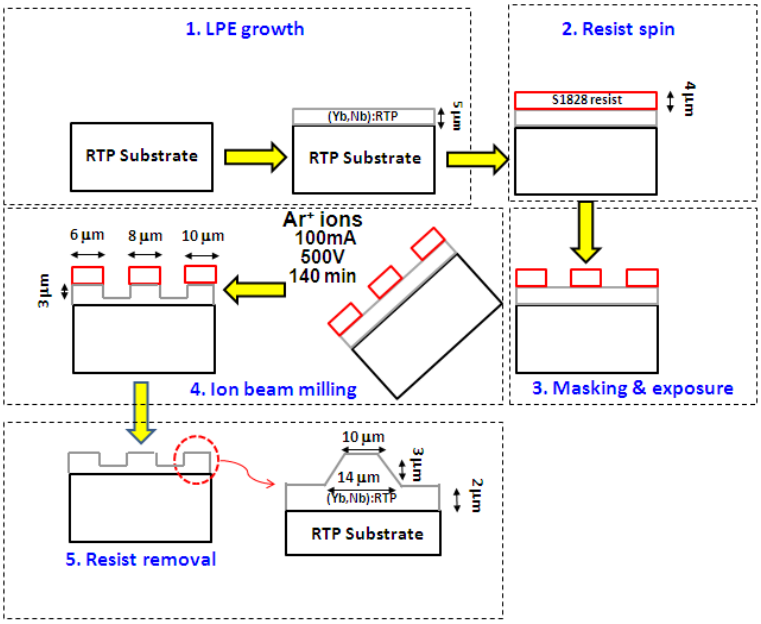

Fig. 1. Schematic diagram of the surface rib waveguide fabrication.

The substrate was included in glue on a glass slide in order to remove any edge effects for the following photolithographic process. A 4-µm-thick layer of S1828 resist was spin-coated onto the sample before masking and development. A dark field mask was used with waveguide widths from 2 µm to 10 µm, with a separation of 100 µm between them. The dark field mask channels were carefully aligned along the ***a*** crystallographic direction of the substrate in order to produce ribs on it parallel to this direction. As can be

#194568 - $15.00 USD Received 25 Jul 2013; revised 26 Sep 2013; accepted 28 Sep 2013; published 21 Oct 2013

seen in Table 1, the refractive index contrast between the doped layer and the undoped substrate is positive for the ***b*** and ***c*** polarizations and negative for the ***a*** polarization. Thus, guiding is possible in TM and TE regimes along ***a*** direction, but only in TM along ***b*** direction. The etching process was carried out in an Oxford Plasma Technology Ionfab 300 Plus system. The masked sample was held at 45° and rotated at 5 rpm during the process. An Ar^+ ion beam was accelerated at 500 V with a beam current of 100 mA. This beam etched the sample for 2 hours and 20 minutes to obtain 3-μm-high ribs in the film. The resist was then removed by acetone and plasma ashing. Figure 1 shows a schematic view of the complete process of rib waveguide fabrication.

3. Results and discussion

A Sensofar PLμ 2300 optical confocal/interferometer microscope was used to check the quality and the dimensions of the ribs. With this microscope the top widths of the ribs were measured and their dimensions ranged from 3 μm to 10 μm, in agreement with the values of the mask used. The profile of the ribs was studied using a non-contact profiler (Zescope by Zemetrics). Figure 2 shows a 3D image of a rib waveguide, demonstrating the good quality of the side-walls.

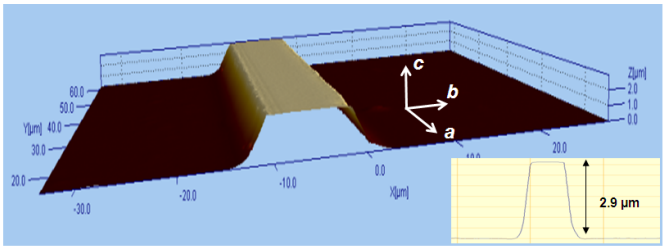

Fig. 2. 3D image obtained with a non-contact profiler of a rib waveguide with a nominal width of 10 μm and its profile in inset.

The rms roughness was measured to be 50 nm on the top and the wall of the side-walls of the ribs. The depth milled was 2.9 μm as can be seen from the inset of Fig. 2. It is important to note that the shape of the rib is not rectangular (see Fig. 2), but is trapezoidal. The end-faces of the waveguides were then polished with the sample sandwiched between two glass blocks to protect the edges. After polishing the end faces we were able to measure the width of the rib base and it was found to be 4 μm larger than the width at the top, indicating that the slope of the rib walls was 34 degrees off vertical. Figure 3(a) is a general view of the ribs in a top-view regime using an Environmental Scanning Electron Microscope (ESEM). In a more detailed view, Fig. 3(b) shows a rib of 9 μm in width and the good quality of the rib walls is qualitatively confirmed. The length of ribs after end-faces polishing process was 6 mm.

As the ESEM microscopy characterization reveals, the rib walls obtained by Ar^+ ion milling were not vertical. Therefore, a simulation using the real parameters was carried out in order to check the degree of expected optical confinement. The dimensions of the ribs simulated were between 3 and 10 μm at the top and between 7 and 14 μm at the base, all of them with symmetrical trapezoidal shape. The simulation shows values of the confinement factor of 88.5% and 93.1% for ribs of 3 μm and 10 μm in width, respectively. So, it reveals a theoretical high confinement, even for the ribs with lower cross section area.

#194568 - $15.00 USD Received 25 Jul 2013; revised 26 Sep 2013; accepted 28 Sep 2013; published 21 Oct 2013

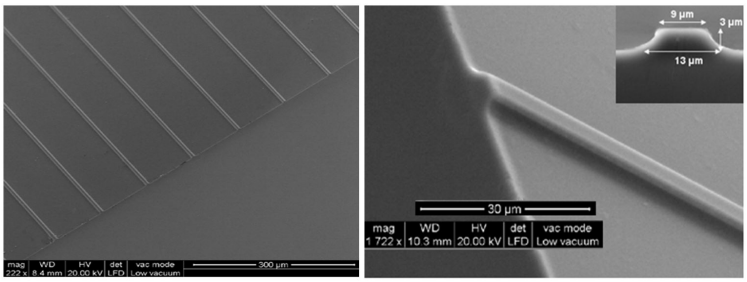

Fig. 3. a) General top view of the rib waveguides by Environmental Scanning Electron Microscope (ESEM) and b) detailed view of the 9 µm nominal width rib waveguide by ESEM, with cross section view in inset.

In order to estimate the transmission losses of the channel waveguides, a 10x objective microscope was used to couple the 972 nm laser beam into the rib waveguide. Using an x-y-z translation stage and optimized launching conditions it was possible to excite only the fundamental mode. Finally, a 50x microscope objective was used to collect the transmitted light. To estimate the transmission losses, the beam power was measured before the input microscope objective, as well as, after the output microscope objective. The single-pass transmission losses were calculated using the expression Loss = $(-10/d)*\log(P_{out}/P_{in})$, where P_{out} is the power at the end of the channel waveguide, P_{in} is the power launched into the channel waveguide and *d* is the waveguide length. Fresnel losses (9%), the transmission of the microscope objectives (46% and 52% for input and output objectives, respectively), the Yb^{3+} absorption (20%) and the launch efficiency (19% and 23%) were taken into account in order to calculate P_{in} and P_{out} from the measured values. The output power from the sample that was not guided was filtered with a motorized diaphragm before the output microscope objective. By applying these corrections and using the expression mentioned above, we estimated an upper limit of the transmission losses of 0.3 dB/cm.

The near-field pattern was measured in order to understand the energy distribution of the propagation modes for the pump wavelength. The experimental set up was the same as that used for the loss measurement, except that in this case a CCD camera was put behind the output objective microscope to observe the image of the output facet of the rib waveguides. A Ti:Sapphire laser at 972 nm was coupled into the waveguide, and the modes in the TM polarization were observed. Figure 4 shows the near-field pattern of the rib of 10 µm in top-width. This figure shows the good agreement between the simulated profile of the TM fundamental mode and the real profile, but the camera response is saturated. A high optical density filter was used to record a non-saturated profile of the mode as is shown in the inset of Fig. 4. As expected, the mode is asymmetric, with near-Gaussian profiles with $1/e^2$ beam radii of ~8.5 µm and ~3.5 µm in the *b* and *c* directions respectively.

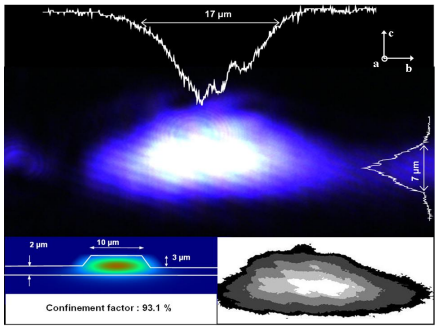

Fig. 4. Near-Field Pattern (NFP) of the fundamental mode at 972 nm of the 10 µm top width rib. The simulation result and the distribution of energy are shown in the lower part.

#194568 - $15.00 USD Received 25 Jul 2013; revised 26 Sep 2013; accepted 28 Sep 2013; published 21 Oct 2013

Second Harmonic Generation (SHG) inside the rib waveguide was checked using a pulsed laser from an optical parametric oscillator (OPO) (Vibrant HE 355 II + UV model from Opotech company) coupled to the rib waveguides by a microscope objective. The OPO was tuned to obtain maximum efficiency of SHG for propagation along the ***a*** crystallographic direction. An achromatic half-wave plate was placed between the laser source and the sample at an angle of 22.5° to ensure that the TM and TE modes were excited simultaneously, which is required for type II SHG. The guided green light, obtained exclusively inside the channels, was collected and imaged onto a CCD camera. Figure 5 shows the 570 nm green light obtained from type II SHG in a rib of 10 μm top-width. The fundamental wavelength was 1140 nm. The accuracy in the wavelength measurements was 0.5 nm. In order to check that the 570 nm light was coming exclusively from the rib waveguide we focused the OPO beam through the substrate, obtaining non guided light, and then we tuned the laser obtaining a maximum of frequency conversion at 1137 nm. Note that this value is different to that obtained inside the rib, which is logical taking into account that the effective refractive indices of the waveguide are different to the refractive indices of the bulk, and in addition the chemical composition of the bulk and the epitaxy are different. The phase matching wavelength obtained in the guided light is bigger than the one in the substrate, in agreement with the results published by Risk et al. [19] for KTP. As can be seen in Fig. 5, the efficiency of type II SHG in the waveguide is significantly higher than in the substrate. Accurate evaluation of the SHG efficiency as a function of I(ω) will be matter of an extended future study.

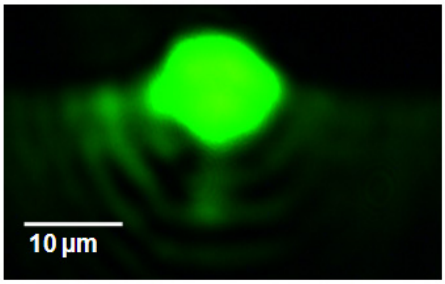

Fig. 5. CCD image of 570 nm green light from type II SHG of 1140 nm IR light, parallel to the ***a*** crystallographic direction.

4. Conclusion

We have reported, for the first time, microstructured rib waveguides on (Yb,Nb):RTP/RTP active planar waveguides. An initial simulation revealed that rectangular ribs with 10 μm width have optical confinement as high as 92.9%. Experimentally, after microstructuring planar waveguides, we found that the shape of the ribs was trapezoidal, and the simulations with real parameters showed confinements of 93.1% for ribs with a 10 μm top-width. A single pass transmission measurement was used to estimate the losses of the rib waveguides, showing losses of 0.3 dB/cm. Type II second harmonic generation was demonstrated by exciting both, TE and TM modes simultaneously at a wavelength of 1140 nm, obtaining 570 nm green light.

Acknowledgments

This work was supported by the Spanish Government under projects TEC2010-21574-C02-02, MAT2011-29255-C02-02, and the Catalan Authority under project 2009SGR235. This work has been partially funded by the European Commission under the Seventh Framework Programme, under project Cleanspace, FP7-SPACE-2010-1–GA-263044. This work was also supported by the U.K. EPSRC under project EP/H035745/1. J. Cugat thanks the Spanish Government for the FPI fellowship BES-2009-024190. A.Choudhary acknowledges N.Sessions and D.Sager for technical support in the ORC cleanrooms.

#194568 - $15.00 USD Received 25 Jul 2013; revised 26 Sep 2013; accepted 28 Sep 2013; published 21 Oct 2013